Noname manuscript No.
(will be inserted by the editor)

A Model for Lubricant Transfer from Media to Head during Heat Assisted Magnetic Recording (HAMR) Writing

Siddhesh V. Sakhalkar · David B. Bogy

Received: date / Accepted: date

Abstract One of the challenges in Heat Assisted Magnetic Recording (HAMR) is the creation of write- induced head contamination at the near field transducer (NFT). A possible mechanism for the formation of this contamination is the transfer of lubricant from the disk to the slider (lubricant pick-up) due to temperature driven evaporation/ condensation and/or mechanical interactions. Here we develop a continuum model that predicts the head to disk lubricant transfer during HAMR writing. The model simultaneously determines the thermo-capillary shear stress driven deformation and evaporation of the lubricant film on the disk, the convection and diffusion of the vapor phase lubricant in the air bearing and the evolution of the condensed lubricant film on the slider. The model also considers molecular interactions between disk - lubricant, slider - lubricant and lubricant - lubricant in terms of disjoining pressure. We investigate the effect of media temperature, head temperature and initial lubricant thickness on the lubricant transfer process. We find that the transfer mechanism is initially largely thermally driven. The rate of slider lubricant accumulation can be significantly reduced by decreasing the media temperature. However, as the amount of lubricant accumulation increases with time, a change in the transfer mechanism occurs from thermally driven to molecular interactions driven. A similar change in transfer mechanism is predicted as the head disk spacing is reduced. There exists a critical value of head lubricant thickness and a critical head disk spacing at which dewetting of the disk lubricant begins, leading to enhanced pick-up.

Keywords Hard disk drives · Heat Assisted Magnetic Recording (HAMR) · Lubricant · Disjoining Pressure · Evaporation · Contamination · Smear

S. V. Sakhalkar (✉) · D. B. Bogy
Computer Mechanics Laboratory, Department of Mechanical Engineering, University of California at Berkeley, Berkeley, CA 94720, USA
Tel.: +1-650-4574999
E-mail: siddhesh_sakhalkar@berkeley.edu

1 Introduction

Heat Assisted Magnetic Recording (HAMR) is widely viewed as a technology that is essential to achieve storage densities beyond 1 Tb/in^2 in hard disk drives [1]. However, reliability of the head-disk interface (HDI) during high temperature transient laser heating still remains a major challenge that needs to be addressed before HAMR can be made into a robust commercial product [2]. One of the tribological challenges in HAMR is the formation of write-induced head contamination at the near field transducer (NFT) [3]. This contamination forms only when the head NFT is energized and the media is heated to its Curie temperature. Kiely et. al. [3] reported measurements of contamination thickness as a function of write time for a variety of different heads in different operating conditions. They observed that the contamination begins very quickly after the laser power is turned on (less than 1 second) and grows over time until the contamination height reaches the head-disk clearance. Once the head contamination contacts the media surface, the disk motion generates a smear down-track of the NFT.

One possible mechanism that has been proposed for HAMR contamination is lubricant desorption from the disk and adsorption on the head through thermodynamic driving forces [3]. During HAMR, the media is locally heated to its Curie temperature ($\sim$ 500 °C). The head also locally reaches a high temperature due to

the NFT and back-heating from the disk, however, the peak temperature of the head is lower than that of the disk ($\sim$ 310 ^{o}C) [3]. This temperature difference causes the lubricant to evaporate from the disk and condense on the relatively cooler head. The lubricant acts as a carrier, causing a continuous deposition of contaminants originating from the media at the head NFT. Alternatively, the contaminants themselves may be desorbed and adsorbed by a similar thermodynamic mechanism. Either way, once the contaminants are deposited on the NFT, they possibly undergo thermo-chemical reactions (pyrolysis) at high temperature, leaving a non-volatile residue on the NFT.

Xiong et. al. [4] also reported deposition of materials on the head after HAMR writing. They observed that after the NFT was turned off and the head-media temperature difference was inverted, material was transfered from the head back to the media. This indicates that the temperature difference between the head and the media is one important mechanism for the material transfer. However, they also reported that the trace of the head deposits lasts about 1 μs, which is close to the mechanical transient of the NFT protrusion, but longer than the thermal response of the head and media. Thus mechanical interaction is an additional mechanism leading to material transfer from the media to the head.

Understanding the mechanism of disk to head lubricant and contaminant transfer is crucial in order to eliminate or control its effect and to develop reliable HAMR drives. There have been several studies on transfer of perfluoropolyether (PFPE) lubricant from the disk to the slider due to evaporation/condensation for non-HAMR drives [5] [6] and HAMR drives [7] [8]. Ma and Liu [7] studied the effect of disk temperature and lubricant molecular weight on lubricant depletion and head transfer in HAMR. However, their model assumed a uniform disk lubricant film and a uniform temperature distribution, ignoring the effect of spatial temperature gradient on lubricant evolution. Yang et. al. [8] reported lubricant accumulation on the media surface after the laser was turned off. They proposed a simple lubricant equilibrium model assuming uniform temperatures and lubricant thicknesses to explain their results.

Existing continuum models for head-disk lubricant transfer by evaporation/condensation have involved oversimplifications and have not been able to quantitatively predict the actual disk-to-slider lubricant transfer process in HAMR. Wu [9] developed a model to predict the lubricant transfer from the head to the disk considering coupled-evaporation condensation and migration dynamics. In that study, a model was proposed that can predict the lubricant partial vapor phase distribution within the air bearing layer, which is imperative to quantitatively describe the disk to slider lubricant transfer. That study was performed for non-HAMR drives and the evolution of the disk lubricant profile was not considered.

There have been several studies on lubricant transfer from the disk to the slider caused by mechanical interactions. Ambekar et. al. [10] reported experimental data suggesting the existence of a critical clearance between the head and disk below which significant lubricant transfer takes place. They explained this phenomenon through a disjoining pressure model that accounts for the influence of the slider to predict the onset of dewetting. Other studies have also used similar disjoining pressure models considering disk-lubricant, slider-lubricant and lubricant-lubricant interactions in order to explain lubricant instability at low clearances [11] [12] [13] [14]. Both temperature difference driven evaporation/ condensation and molecular interactions based mechanical transfer are important mechanisms causing lubricant transfer in HAMR and the influence of both of these must be considered in order to predict the lubricant transfer process.

The evolution of the disk lubricant film under HAMR laser illumination has been well studied. Continuum as well as molecular dynamics models have been developed to predict the lubricant profile under the influence of the driving forces including surface tension gradient, disjoining pressure, evaporation and thin film viscosity [15] [16] [17] [18]. While the effects of dispersive and polar disjoining pressure for different PFPE lubricants have been studied [19], the effects of the slider and slider lubricant on the disjoining pressure have not been modeled. The migration of the slider lubricant film caused by air shear stress and pressure has also been studied [20]. However, to our knowledge, there is no existing continuum model that considers the deformation of the disk lubricant film under HAMR heating while predicting the lubricant transfer process. The evolution of the deposited lubricant film on the slider under the temperature gradient at the NFT has also not been studied.

During HAMR writing, there is a continuous circulation of lubricant between the disk, the air bearing and the slider. The depletion and deformation of disk lubricant, diffusion and convection of the vapor phase and the evolution of the deposited slider lubricant are strongly coupled and must be modeled simultaneously to understand the physics of the transfer process. In this study, we develop a model that predicts the evolution of the disk lubricant film, the lubricant vapor phase in the air bearing and the slider lubricant layer during HAMR writing. We investigate the effects of media temperature, head temperature and initial lubricant thickness on the lubricant transfer process. We also study the effects of

slider-lubricant and lubricant-lubricant molecular interactions on the disk-to-head lubricant transfer.

2 Lubricant Model

During HAMR writing, the media is locally heated to its Curie Temperature ($T_{max,d} \sim 500^oC$). The high spatial temperature gradient (∇T_d) causes the lubricant film on the disk (thickness h_d) to deform and evaporate. Lubricant evaporation causes the partial pressure of the lubricant vapor in the air bearing, p_v to rise. Some of this lubricant vapor condenses on the relatively cooler slider surface (maximum head temperature $T_{max,s} \sim 310^oC$) [3], depositing a thin lubricant film of thickness h_s. The spatial temperature gradient on the slider (∇T_s) causes this deposited lubricant film to deform. A schematic of this disk to slider lubricant transfer process is shown in Figure 1. Thus, we have three unknowns in this problem - $h_d(x,y,t)$, $h_s(x,y,t)$ and $p_v(x,y,t)$. In this study we apply this simulation tool to the PFPE lubricant Zdol 2000.

The governing equation for the disk lubricant according to lubrication theory is [21]:

$$\frac{\partial h_d}{\partial t} + u_d\frac{\partial h_d}{\partial x} + \frac{\partial}{\partial x}\left[-\frac{h^3}{3\mu}\frac{\partial p_d}{\partial x} + \frac{h_d^2}{2\mu_d}\frac{\partial \tau_{x,d}}{\partial x}\right] + \frac{\partial}{\partial y}\left[-\frac{h^3}{3\mu}\frac{\partial p_d}{\partial y} + \frac{h_d^2}{2\mu_d}\frac{\partial \tau_{y,d}}{\partial y}\right] + \frac{\dot{m}_d}{\rho} = 0 \quad (1)$$

where h_d is the unknown disk lubricant thickness, u_d is the disk velocity in the down-track x direction, μ_d is the effective lubricant viscosity, p_d is the lubricant pressure, $\tau_{x,d}$ and τ_{y_d} are the lubricant shear stress components in the x (down-track) and y (cross-track) directions respectively, ρ is the constant lubricant density and $\dot{m}_d$ is the mass flux due to evaporation from the disk.

2.1 Surface Tension

The resultant stress due to surface tension can be decomposed into two components. The first component called Laplace Pressure acts normal to the lubricant surface due to surface curvature and is given by:

$$p_{lap}\boldsymbol{n} = (-\gamma\nabla\cdot\boldsymbol{n})\boldsymbol{n} = \gamma\nabla^2 h$$

Previous studies by Dahl and Bogy [15] and Sarabi and Bogy [19] have shown that the effect of the Laplace Pressure on lubricant evolution under HAMR is negligible, particularly for thin lubricant films ($\leq$ 1.2 nm). Hence, in this study, the effect of Laplace pressure on the lubricant evolution is ignored.

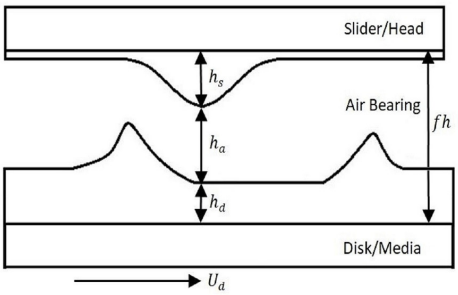

Fig. 1: HAMR Lubricant Transfer Schematic: Disk Lubricant of thickness $h_d(x,y,t)$ is subjected to a scanning laser spot of speed u_d. The disk lubricant evaporates to form vapor having partial pressure $p_v(x,y,t)$ in the HDI. The vapor condenses on the slider to form a film of thickness $h_s(x,y,t)$.

The second component called Maragoni Stress [22] acts tangential to the lubricant surface due to spatial non-uniformity of surface tension. In this application, the variation in surface tension is due to the temperature gradient (also called "thermocapillary shear stress") and can be expressed as:

$$\boldsymbol{\tau} = \nabla\gamma - (\nabla\gamma\cdot\boldsymbol{n})\boldsymbol{n} = \gamma\nabla^2 h$$

With the quasi-parallel film assumption ($|\nabla h| \ll 1$,$\boldsymbol{n} \approx \boldsymbol{e_z}$), the resultant shear stress on the disk lubricant can be expressed as:

$$\boldsymbol{\tau_d} = \frac{\partial\gamma}{\partial x}\boldsymbol{e_x} + \frac{\partial\gamma}{\partial y}\boldsymbol{e_y} = -c\left(\frac{\partial T_d}{\partial x}\boldsymbol{e_x} + \frac{\partial T_d}{\partial y}\boldsymbol{e_y}\right) \quad (2)$$

Here, $c \equiv -\frac{d\gamma}{dT}$ is assumed to be constant and equal to 0.06 $mN/(m^oC)$ for Zdol 2000 [15].

2.2 Disjoining Pressure

The concept of Disjoining Pressure was introduced by Derjaguin [23] and defined as the difference between the normal component of the pressure tensor in the liquid film and that of the bulk phase of the same liquid under the same thermodynamic conditions. For a one-component liquid, the disjoining pressure may be determined as the derivative of the free energy per unit area of a thin layer, which arises from the effect of surface forces. Based on this definition, some researchers have tried to obtain appropriate expressions for the disjoining pressure of PFPE lubricants [24] [25] according to the following equation:

$$\Pi_d(h_d) = -\frac{\partial\gamma_d^d}{\partial h_d} - \frac{\partial\gamma_d^p}{\partial h_d} = \Pi_d(h_d)^d + \Pi_d(h_d)^p = \frac{A_{VLS}}{6\pi(h_d+d_0)^3} + \Pi_d(h_d)^p$$

Here we consider two components of disjoining pressure and use the mischaracterizing nomenclature common in hard drive lubricant literature [11] - dispersive Π_d^d and polar Π_d^p, based on the corresponding components of the thin film surface energy γ_d^d and γ_d^p. The dispersive disjoining pressure Π_d^d is a consequence of van der Waals interactions and has a $1/h^3$ dependence. Here A_{VLS} is the Hamaker constant for the vapor-liquid-solid system. d_0 is a constant introduced to account for the molecular effect of the finite size of the atoms and molecules within the lubricant film. The oscillating polar component Π_d^p is due to structural effects or non-van der Waals interactions introduced by the functional end-groups and is typically represented by a polynomial expansion. The coefficients of dispersive disjoining pressure ($A_{VLS} = 4.59 \times 10^{-20}$ J, $d_0 = 0.172$ nm) and polar disjoining pressure (curve-fitting parameters for polynomial expansion) of Zdol 2000 can be found in the paper by Sarabi and Bogy [19]. These coefficients are based on the methodology described by Karis and Tyndall [24] and the experimental data of surface energy of unannealed Zdol 2000 given by Tyndall et. al. [25].

Some researchers [11] have questioned the assumptions made in the widely used contact angle method used to determine disjoining pressure in [24], [25]. While such methods seem to provide reasonable estimates of surface energies for solid surfaces, it has been cautioned that the values determined for disjoining pressure should not be taken as a true experimental measurement. In the absence of an accurate method for measuring disjoining pressure for actual lubricant/disk systems, we also use the contact angle measurements in [25].

At nanometer scale head-disk clearances, the disk lubricant disjoining pressure is also influenced by the presence of the slider and the lubricant layer on the slider. Several previous works [26], [10] and [11] consider the influence of the slider on the disk lubricant disjoining pressure, while ignoring the liquid-liquid interactions. However, as the amount of lubricant accumulation on the slider increases, the liquid-liquid interactions can no longer be neglected. The resulting expression for the disk lubricant disjoining pressure is given by: [27], [28], [29]

$$\Pi_d(h_d, h_s) = \frac{A_{VLS}}{6\pi(h_d + d_0)^3} + \Pi_d(h_d)^p + \frac{A_{VLS}}{6\pi(fh - h_d - d_0)^3} + \frac{A_{LVL}}{6\pi(fh - h_d - h_s - 2d_0)^3} \quad (3)$$

Here A_{LVL} is the Hamaker constant for the liquid-liquid interactions through vapor. In this study, we assume that $A_{LVL} \approx (2.1 \times 10^{-18})\gamma_\infty \approx 3 \times 10^{-20}$ J [30] [26], where $\gamma_\infty = 15.8 \times 10^{-3}\ J/m^2$ is the bulk surface energy of Zdol 2000. A detailed derivation of Eq. (3) can be found in [28]. It is worthwhile to note that in the characterization of disjoining pressure in Eq. (3), we define Hamaker constants such that $A_{VLS} > 0$ and $A_{LVL} > 0$. Defining A_{SVL} as the Hamaker constant for solid-liquid interactions through vapor and assuming $A_{SVL} \approx A_{VLS} + A_{LVL}$ [26], Eq. (3) can be equivalently expressed as:

$$\Pi_d(h_d, h_s) = \left[\frac{A_{VLS}}{6\pi(h_d + d_0)^3} + \Pi_d(h_d)^p\right] + \left[\frac{A_{SVL}}{6\pi(fh - h_d - d_0)^3}\right] + \left[\frac{A_{LVL}}{6\pi(fh - h_d - h_s - 2d_0)^3} - \frac{A_{LVL}}{6\pi(fh - h_d - d_0)^3}\right] \quad (4)$$

In Eq. (4), the first term represents the disjoining pressure of the disk lubricant due to van der Waals and polar interactions with the disk, the second term represents the influence of the slider on the disk lubricant disjoining pressure and the third term represents the influence of the slider lubricant film on the disk lubricant disjoining pressure. The expression for disjoining pressure found in [26], [10] and [11] is the same as Eq. (4), if we ignore the last term (liquid-liquid interaction).

2.3 Thin Film Viscosity

Karis [31] applied Eyring's rate theory to develop a thin film viscosity model for hard disk drive lubricants and gave the following equation:

$$\mu_d(h_d) = \frac{N_A h_P}{V_l} exp\left(\frac{\Delta E_{vis}(h_d) - T_d \Delta S_{vis}(h_d)}{RT_d}\right) \quad (5)$$

where N_A is Avogadro's number, h_P is Planck's constant, V_l is the molar volume of the lubricant, $\Delta E_{vis}(h_d)$ is the film thickness dependent flow activation energy, $\Delta S_{vis}(h_d)$ is the film thickness dependent flow activation entropy, R is the universal gas constant and T_d is the disk lubricant temperature. We use the same $\Delta E_{vis}(h_d)$ and $\Delta S_{vis}(h_d)$ values as those found in [31] for Zdol [15].

2.4 Evaporation

Dahl and Bogy [15] used the method of Karis [32] to calculate the bulk vapor pressure of Zdol $p_{vap,\infty}(T, M_w)$ with the Clapeyron equation and ideal gas law. With the bulk vapor pressure known, the equilibrium thin film vapor pressure is determined using the following expression [33]:

$$\frac{p_{vap,film}(h_d, h_s)}{p_{vap,\infty}} = exp\left(\frac{M_w}{\rho RT_d}[-\pi_d(h_d, h_s)]\right) \quad (6)$$

Next, the net evaporation rate is determined using the Hertz-Knudsen-Langmuir model [34] as:

$$\dot{m}_d(h_d, h_s, p_v) = \alpha\sqrt{\frac{M_w}{2\pi R T_d}}(p_{vap,film}(h_d, h_s) - p_v) \quad (7)$$

where $\dot{m}_d$ is the net evaporation mass flux from the disk, M_w is the lubricant molecular weight, R is the molar universal gas constant, T_d is the disk lubricant temperature and α is the accommodation constant (assumed to be 1 in this study). $p_{vap,film}$ is the equilibrium thin film vapor pressure and p_v is the partial pressure of the lubricant vapor in the air bearing. Previous works on lubricant deformation under HAMR conditions [15] [19] [16] [17] have assumed p_v to be 0. However, when the media is heated to its Curie temperature, significant evaporation of the lubricant is expected to occur. As a result, the partial pressure of the lubricant vapor in the air bearing can not be ignored and must be studied using a separate evolution equation. This equation will be discussed in subsequent sections (2.7 - 2.9).

2.5 Governing Equation for the Disk Lubricant

The governing equation for the disk lubricant can be obtained by substituting Eq. (2), (3), (5) and (7) in Eq. (1):

$$\begin{aligned}\frac{\partial h_d}{\partial t} + u_d\frac{\partial h_d}{\partial x} + \frac{\partial}{\partial x}\left[\frac{h_d^3}{3\mu_d}\frac{\partial \pi_d}{\partial x} - \frac{h_d^2}{2\mu_d}c\frac{\partial T_d}{\partial x}\right] \\ + \frac{\partial}{\partial y}\left[\frac{h_d^3}{3\mu_d}\frac{\partial \pi_d}{\partial y} - \frac{h_d^2}{2\mu_d}c\frac{\partial T_d}{\partial y}\right] + \frac{\dot{m}_d}{\rho} = 0\end{aligned} \quad (8)$$

In this study, we have ignored the effect of the air bearing pressure and shear stress on the disk to slider lubricant transfer process. The timescale of this transfer process is of the order of nanoseconds, while the effects of the air bearing pressure and shear stress are expected to be on the order of seconds [35] [16].

We use the same non-dimensionalization scheme as Dahl and Bogy [15].

$$\begin{aligned} h_d* = h_d h_{0,d} \quad x* = xL \quad y* = yL \\ \mu* = \mu_0\mu \quad T_d* = T_d\Delta T_d + T_0\end{aligned} \quad (9)$$

Here $h_{0,d}$ is the initial disk lubricant thickness, L is the disk temperature profile FWHM, T_0 is the ambient temperature, ΔT_d is the maximum prescribed disk temperature rise $T_{max,d} - T_0$ and $\mu_0 = \mu(T_0, h_{0,d})$. This choice of non-dimensional variables implies the following scales and coefficients:

$$\begin{aligned} t* = tt_s \quad \pi_d* = \pi_d p_s \quad t_s \equiv \frac{2\mu_0 L^2}{h_{0,d}c\Delta T_d} \\ p_s \equiv \frac{3}{2}\frac{c\Delta T_d}{h_{0,d}} \quad C_u \equiv \frac{2\mu_0 L u_d}{h_{0,d}c\Delta T_d} \quad S \equiv \frac{2\mu_0 L^2}{h_{0,d}^2 c\Delta T_d}\end{aligned} \quad (10)$$

We now switch to a notation where quantities with an asterisk are dimensional and quantities without an asterisk are non-dimensional. The final non-dimensional governing equation for the disk lubricant is:

$$\begin{aligned}\frac{\partial h_d}{\partial t} + C_u\frac{\partial h_d}{\partial x} + \frac{\partial}{\partial x}\left[\frac{h_d^3}{\mu_d}\frac{\partial \pi_d}{\partial x} - \frac{h_d^2}{\mu_d}c\frac{\partial T_d}{\partial x}\right] \\ + \frac{\partial}{\partial y}\left[\frac{h_d^3}{\mu_d}\frac{\partial \pi_d}{\partial y} - \frac{h_d^2}{\mu_d}c\frac{\partial T_d}{\partial y}\right] + S_d = 0\end{aligned} \quad (11)$$

The initial condition is a uniform film of lubricant of prescribed thickness $h_{0,d}$. We use Neumann boundary conditions on the ends of our domain.

2.6 Governing Equation for the Slider Lubricant

Similarly, the final non-dimensional governing equation for the slider lubricant can be expressed as:

$$\begin{aligned}\frac{\partial h_s}{\partial t} + \frac{\partial}{\partial x}\left[\frac{h_s^3}{\mu_s}\frac{\partial \pi_s}{\partial x} - \frac{h_s^2}{\mu_s}c\frac{\partial T_s}{\partial x}\right] \\ + \frac{\partial}{\partial y}\left[\frac{h_s^3}{\mu_s}\frac{\partial \pi_s}{\partial y} - \frac{h_s^2}{\mu_s}c\frac{\partial T_s}{\partial y}\right] + S_s = 0\end{aligned} \quad (12)$$

The initial condition is a uniform film of lubricant of thickness $h_{0,s}$. We use Neumann boundary conditions on the ends of our domain. It is worthwhile to highlight that h_s is nondimensionalized with respect to $h_{0,d}$ and T_s is non-dimensionalized with respect to ΔT_d. Also, we assume that the FWHM of disk and slider temperature profiles are the same and equal to L.

2.7 Lubricant Vapor in the Air Bearing

Consistent with the lubrication approximation, we assume that the density of the lubricant vapor in the air bearing ρ_v is independent of the normal co-ordinate z, i.e., $\rho_v \equiv rho_v(x, y)$. The governing equation for the lubricant vapor can be obtained by integrating the continuity equation along the normal co-ordinate z and applying Fick's Law of Diffusion [9].

$$\begin{aligned}\frac{\partial}{\partial t}(\rho_v h_a) + \frac{\partial}{\partial x}(\rho_v q_x) + \frac{\partial}{\partial y}(\rho_v q_y) = \\ \frac{\partial}{\partial x}\left(Dh_a\frac{\partial \rho_v}{\partial x}\right) + \frac{\partial}{\partial y}\left(Dh_a\frac{\partial \rho_v}{\partial y}\right) + \dot{m}_d + \dot{m}_s\end{aligned} \quad (13)$$

In this equation, $h_a(h_s, h_d) \equiv (fh - h_s - h_d)$ is the height of the air bearing where fh is the constant head-disk spacing at the NFT (Refer Figure 1). $q_x \equiv \int_{h_d}^{h_d+h_a} v_{a,x}dz$ and $q_y \equiv \int_{h_d}^{h_d+h_a} v_{a,y}dz$ are the volume flow rates per unit length in the x and y directions, obtained by integrating the air bearing velocity $v_{a,x}$ and $v_{a,y}$ in the

z direction across the air bearing clearance. D is the lubricant vapor diffusivity in air and $\dot{m}_d$ and $\dot{m}_s$ are the net evaporation mass fluxes from the disk and slider lubricant films respectively. Eq. (13) also assumes that the lubricant vapor in air is a dilute mixture so that the binary mixture velocity can be approximated by the air bearing velocity $v_{m,x} \approx v_{a,x}$ and $v_{m,y} \approx v_{a,y}$ and that the mixture density ρ_m is approximately constant over the scale on which ρ_v varies.

The first term in Eq. (13) models the unsteady lubricant vapor density change and dynamic air bearing height change. The next two terms on the LHS of Eq. (13) model the vapor convection effect due to the air bearing velocity. The effect of lubricant vapor diffusion in the air bearing layer is modeled by the first two terms on the RHS of (13). Finally, lubricant evaporation/condensation from the disk/slider is modeled by the last two terms of Eq. (13).

In this study, we assume that the effects of the lubricant vapor on the air bearing pressure, temperature and velocity can be neglected. Also, the lubricant as well as air bearing temperature is simply assumed to be equal to the average of the disk and slider temperatures $T_v \equiv (\frac{T_s+T_d}{2})$. Finally, the lubricant vapor density and partial pressure are assumed to be related by the ideal gas law:

$$P_v = \frac{\rho_v R T_v}{M_w} \tag{14}$$

where R is the molar universal gas constant and M_w is the lubricant molecular weight.

2.8 Convection and Diffusion

The lubricant convection model in Eq. (13) requires the air bearing velocity profiles in the x and y directions near the location of the NFT. Theoretically, this velocity profile can be obtained from an air bearing model for HAMR like CMLAir HAMR [36]. However, the air bearing model in [36] is rather coarsely meshed near the NFT location. Hence, due to the lack of accurate air velocity profiles very close to the NFT, we assume the following simple model for volume fluxes q_x and q_y:

$$q_x = u_d(fh - h_{0,d} - h_{0,s}) \quad q_y = 0 \tag{15}$$

Karis [32] used the Hirschfelder approximation [37] to obtain the lubricant vapor phase diffusion coefficient:

$$D = 1.858 \times 10^{-4} \left(\frac{1}{M_w} + \frac{1}{M_a}\right)^{0.5} \frac{T_v^{1.5}}{P_a \sigma_i \Omega} \tag{16}$$

where M_a and M_w are the air and lubricant molecular weights and P_a is the air bearing pressure. Expressions for collision diameter σ_i and collision integral Ω can be found in [32].

2.9 Governing Equation for the Lubricant Vapor

We use the following non-dimensionalization for the lubricant vapor equation (13):

$$\begin{aligned} \rho_v* = \rho_v \rho_l \quad h_a* = h_a h_{0,d} \quad q_x* = q_x q_0 \\ q_y* = q_x q_0 \quad D* = D D_0 \\ q_0 \equiv \frac{L h_{0,d}}{t_s} \quad C_D \equiv \frac{t_s D_0}{L^2} \end{aligned} \tag{17}$$

Here ρ_l is the density of the liquid lubricant and D_0 is the diffusivity at ambient temperature T_0 and pressure p_0 ($D_0 \equiv D(T_0, p_0)$). The spatial and temporal non-dimensionalization is the same as that for the disk/slider lubricant Eq. (9) and (10). We now switch to a notation where quantities with an asterisk are dimensional and quantities without an asterisk are non-dimensional. The final non-dimensional governing equation for the lubricant vapor is:

$$\begin{aligned} \frac{\partial}{\partial t}(\rho_v h_a) + \frac{\partial}{\partial x}(\rho_v q_x) + \frac{\partial}{\partial y}(\rho_v q_y) = \\ \frac{\partial}{\partial x}\left(C_D D h_a \frac{\partial \rho_v}{\partial x}\right) + \frac{\partial}{\partial y}\left(C_D D h_a \frac{\partial \rho_v}{\partial y}\right) + S_d + S_s \end{aligned} \tag{18}$$

2.10 Numerical Scheme

Equations (11), (12) and (18) are three coupled partial partial differential equations in the three unknows h_s, h_d and ρ_v (or equivalently P_v through (14)). Equations (12) and (18) are discretized using a finite volume method (Hybrid Scheme) [38]. For the disk lubricant equation (11), we follow the method used by Dahl and Bogy [15] - the non-advective part of the equation is discretized using the Hybrid Scheme and the advective part is solved using the Cubic Interpolation Spline (CIP) scheme [39], [40]. The resulting set of non-linear, coupled algebraic equations are solved iteratively to obtain the three solution profiles.

3 Results

During the HAMR writing process, a complex laser delivery system heats the media locally to its Curie temperature, causing the disk lubricant to deform, evaporate and condense at the NFT location on the slider. We perform simulations to study the evolution of the lubricant film on the disk, the evaporated lubricant vapor in the air bearing and the condensed lubricant film on the slider under write conditions.

3.1 Lubricant Transfer during HAMR

For the baseline simulation, we assume an initially uniform film of Zdol 2000 (M_w = 2 kg/mol) of thickness $h_{0,d}$ = 1.2 nm on the disk. The ambient conditions are assumed to be T_0 = 25 °C and p_0 = 101325 Pa. The disjoining pressure experimental data is valid in the thickness range 0.2-2 nm, hence we assume the initial lubricant thickness on the slider ($h_{0,s}$) to be 0.2 nm. We prescribe a gaussian temperature profile with a peak of 500 °C and FWHM of 20 nm on the disk. The slider temperature profile has the same FWHM but a peak of 310 °C. The head-disk clearance fh is set to 4 nm, so that the initial air bearing height ($h_{a,0}$) is 2.6 nm. We consider a disk speed U_d of 12.5 m/s (correspoding to disk rotational velocity of 5400 RPM and radial distance of 22.215 mm) and a simulation time t_f of 2 ns. The air bearing pressure at the NFT is set to 2.2 MPa. The peak disk/slider temperature, head-disk spacing and air bearing pressure data are approximately based on 15 mW TFC (Thermal Fly Height Control) Power and 2 mW NFT Power simulations using the CML HAMR code [36]. We consider the same slider Air Bearing Surface (ABS) design for the HAMR air bearing simulations as [36].

Figure 2 shows the time evolution of the lubricant profile on the disk and the slider in the cross-track and down-track directions. We see a central trough of depth 0.6 nm and side ridges of height 0.2 nm in the cross-track disk lubricant profile, similar to those seen in previous works [15]. The disk lubricant trough depth does not change much over time, however, the length of the depleted region continues to increase due to the disk motion in the down-track direction. As disk lubricant depletion increases with time, lubricant accumulation on the slider also grows. Starting with a uniform film of 0.2 nm on the slider, the simulation predicts a peak lubricant height of 0.83 nm at the end of 2 ns of illumination.

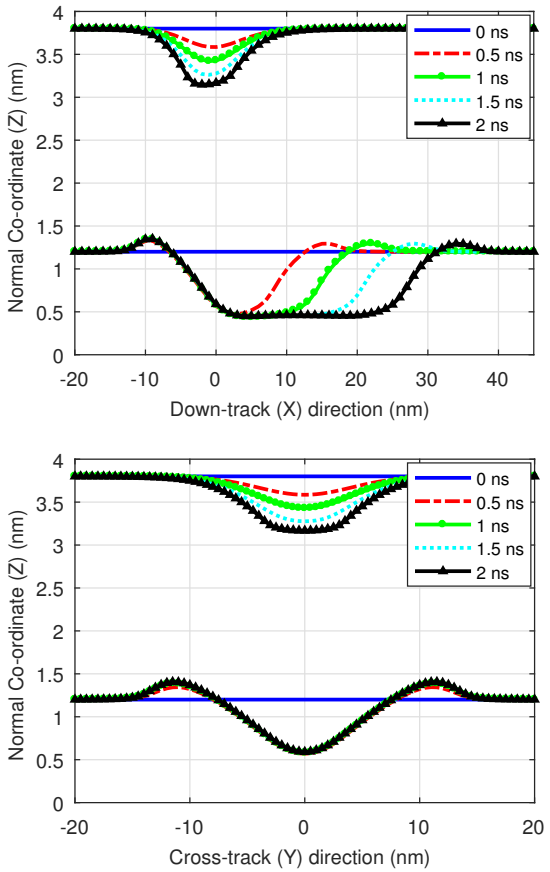

Fig. 2: Cross-track and down-track Lubricant Profile on Disk and Slider at different times of laser illumination. $T_{max,d}$ = 500 °C, $T_{max,s}$ = 310 °C, U_d = 12.5 m/s, fh = 4 nm, FWHM = 20 nm. Origin (X = 0, Y = 0) is at NFT center.

Figure 3 shows the partial pressure of the lubricant vapor in the air bearing in the cross-track direction. The lubricant vapor pressure is less than 0.1 MPa, while the air pressure at the NFT is 2.2 MPa, thereby justifying the dilute vapor assumption. At the NFT location (origin of co-ordinate system), the disk and slider lubricant thicknesses at the end of 2 ns are 0.59 nm and 0.83 nm respectively. The thin film equilibrium vapor pressure (Eq. 6) at film thickness of 0.59 nm (h_d) and temperature of 500 °C (T_d) is 0.3 MPa and at 0.83 nm (h_s) and 310 °C (T_s) is 5 x 10^{-4} MPa. The partial pressure of the lubricant vapor phase at the origin (p_v) is 0.07 MPa. Thus, the large difference between the equilibrium vapor pressure of the disk lubricant and the head lubricant causes this relatively large mass flux from the disk to the head through the air bearing.

Figure 4 shows the dynamic air bearing height ($h_a = fh - h_d - h_s$) in the cross-track direction. At the origin (NFT location), the slider lubricant thickness reaches its peak value, however, the disk lubricant depletion is also maximized here. This causes a local maxima in the air bearing cross-track thickness profile. Two pairs of local minima are seen in the air bearing thickness profile. One pair of minima is seen at y = ± 11 nm, which corresponds to the ridges on the disk lubricant thickness profile. Another pair of minima are seen at y = ± 3.5 nm. This location corresponds to the optimal point for the tradeoff between the rates of disk lubricant depletion and slider lubricant accumulation.

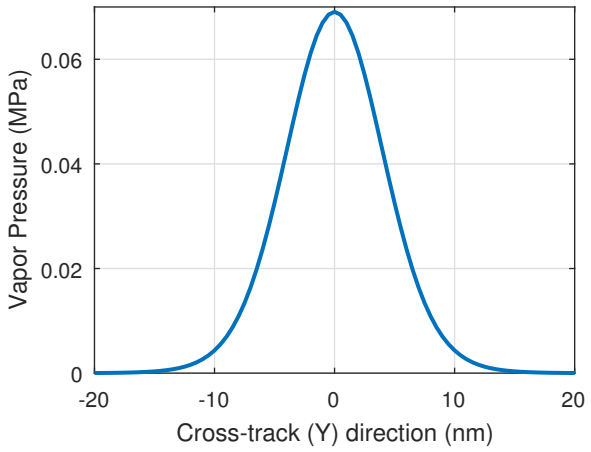

Fig. 3: Cross-track profile of lubricant vapor phase partial pressure at the end of 2 ns of laser shine. $T_{max,d}$ = 500 °C, $T_{max,s}$ = 310 °C, U_d = 12.5 m/s, fh = 4 nm, FWHM = 20 nm. Origin ($X = 0$, $Y = 0$) is at NFT center.

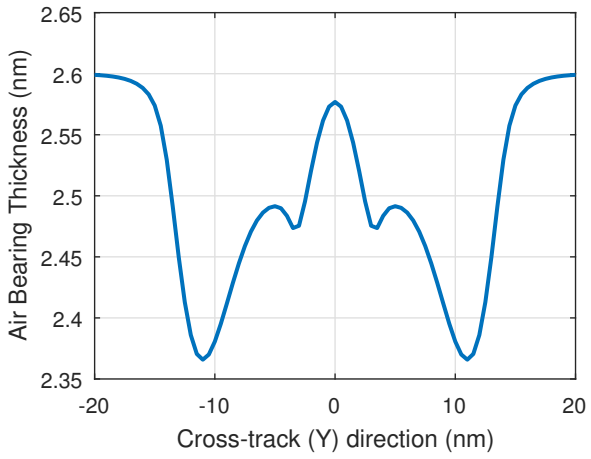

Fig. 4: Cross-track profile of air bearing thickness at the end of 2 ns of laser shine. $T_{max,d}$ = 500 °C, $T_{max,s}$ = 310 °C, U_d = 12.5 m/s, fh = 4 nm, FWHM = 20 nm. Origin ($X = 0$, $Y = 0$) is at NFT center.

3.2 Effect of Disk Temperature

In this section, we investigate how the lubricant transfer process changes with maximum disk temperature, a consequence of varying the laser power, for fixed initial disk and slider lubricant thicknesses of 1.2 nm and 0.2 nm respectively. We illuminate the lubricant with a 20 nm FWHM thermal spot scanning at a speed of 12.5 m/s for 2 ns. The maximum head temperature is kept constant at 310 °C and the maximum disk temperature is varied: 400 °C, 450 °C, 475 °C, 500 °C and 525 °C.

Figure 5 shows the cross-track and down-track profile of the disk and slider lubricant thicknesses for the different disk temperatures. The increase in maximum disk temperature has two effects on the physics of disk lubricant deformation - the rate of evaporation increases and the thermocapillary shear stress becomes stronger (due to higher temperature gradient). At 400 °C, we see some small deformation in the disk lubricant profile, however, there is hardly any accumulation of lubricant on the slider. What little deformation is present at this temperature is due to thermocapillary shear stress. As shown in Figure 5, as the disk temperature is increased, the central trough (caused largely by evaporation) becomes wider as well as deeper. The height of the side ridges caused by thermocapillary shear stress also increases.

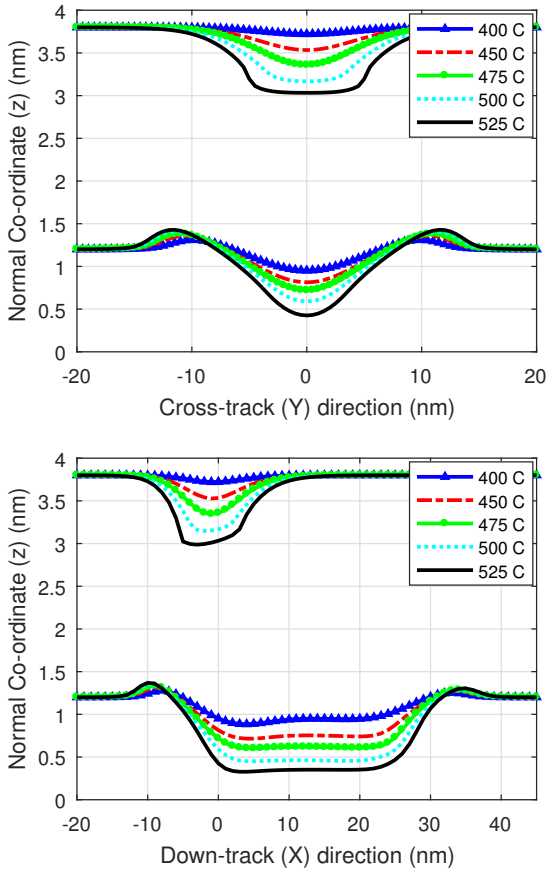

Fig. 5: Cross-track and down-track lubricant profile on the disk and slider at different maximum disk temperatures. Dramatic increase in the slider's lubricant accumulation is predicted with increase in disk temperature. $T_{max,s}$ = 310 °C, U_d = 12.5 m/s, fh = 4 nm, FWHM = 20 nm, t_f = 2 ns. Origin ($X = 0$, $Y = 0$) is at NFT center.

The increased rate of evaporation from the disk causes the lubricant accumulation on the slider to rise.

Figure 8a plots the slider's lubricant accumulation ΔV_{slider} (defined as the difference between the initial and final volume of slider lubricant) as a function of maximum disk temperature. Not only does the lubricant accumulation increase with increase in disk temperature, but the slope of the accumulation versus disk temperature curve also increases at higher temperatures.

3.3 Effect of Slider Temperature

In this section, the maximum disk temperature is kept constant at 500 °C and the maximum slider temperature is varied: 200 °C, 250 °C, 310 °C, 350 °C and 400 °C. All other variables (initial lube thickness, disk speed, laser FWHM, simulation time, head-disk spacing, etc.) are kept the same as in Section 3.2. As shown in Figure 6, change in maximum slider temperature has a minor effect on the disk lubricant profile. As the slider's temperature increases, the amount of lubricant accumulation on the slider decreases, but the effect is relatively small. This is highlighted in Figures 8a and 8b which compare the effects of disk and slider temperatures on the lubricant transfer process. A variation in disk temperature from 400 °C to 525 °C causes the accumulation to increase from a meager 8 nm^3 to 118.8 nm^3. On the other hand, varying the slider's temperature from 200 °C to 400 °C causes only a small change in slider lubricant accumulation from 83.7 nm^3 to 77.9 nm^3.

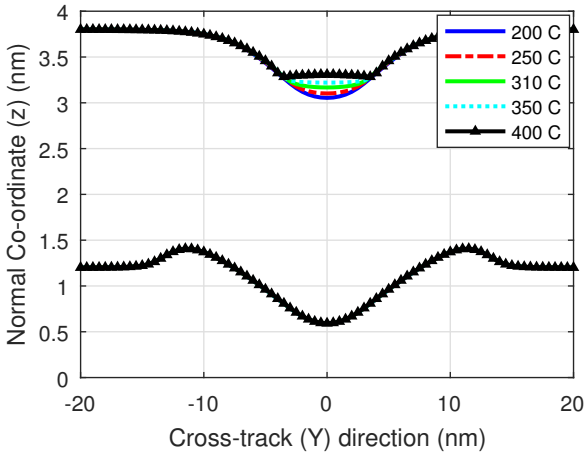

Fig. 6: Cross-track lubricant profile on disk and slider at different maximum Slider Temperatures. $T_{max,d}$ = 500 °C, U_d = 12.5 m/s, fh = 4 nm, FWHM = 20 nm, t_f = 2 ns. Origin ($X = 0$, $Y = 0$) is at NFT center.

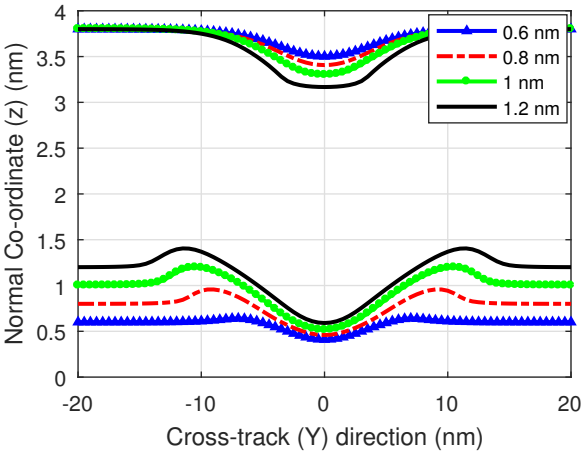

Fig. 7: Cross-track lubricant profile on disk and slider at different initial lube thicknesses. $T_{max,d}$ = 500 °C, $T_{max,s}$ = 310 °C, U_d = 12.5 m/s, fh = 4 nm, FWHM = 20 nm, t_f = 2 ns. Origin ($X = 0$, $Y = 0$) is at NFT center.

3.4 Effect of Initial Lubricant Thickness

Here we study how the lubricant transfer process changes with initial disk lubricant thickness, for fixed disk and slider temperatures. Four cases of disk lubricant thickness: 0.6 nm, 0.8 nm, 1nm and 1.2 nm are considered. Higher lubricant thicknesses are avoided so as to avoid the effect of dewetting and the influence of Laplace pressure. All other variables (initial slider lubricant thickness, disk speed, laser FWHM, simulation time, head-disk spacing, etc.) are kept the same as in Section 3.2. As shown in Figure 7, similar to the maximum disk temperature study, an increase in lubricant thickness causes the depth as well as width of the central trough on the disk to increase. For a disk temperature of 500 °C and slider temperature of 310 °C, thicker lubricant films of 1.2 nm and 1 nm have a peak accumulation thickness of 0.85 nm and 0.71 nm, respectively, while the thinner lubricant films of 0.6 nm and 0.8 nm have a peak accumulation thickness of 0.6 nm and 0.5 nm, respectively. An increased amount and slope (with respect to thickness) of lubricant accumulation on the slider is predicted, as highlighted in Figure 8c.

3.5 Effect of Air Bearing Convection and Diffusion

In this section, we investigate the effect of the air convection and diffusion model described in Section 2.8 on the lubricant transfer process. We illuminate the disk lubricant with a 20 nm FWHM thermal spot scanning at a speed of 12.5 m/s for 1 ns. The maximum disk

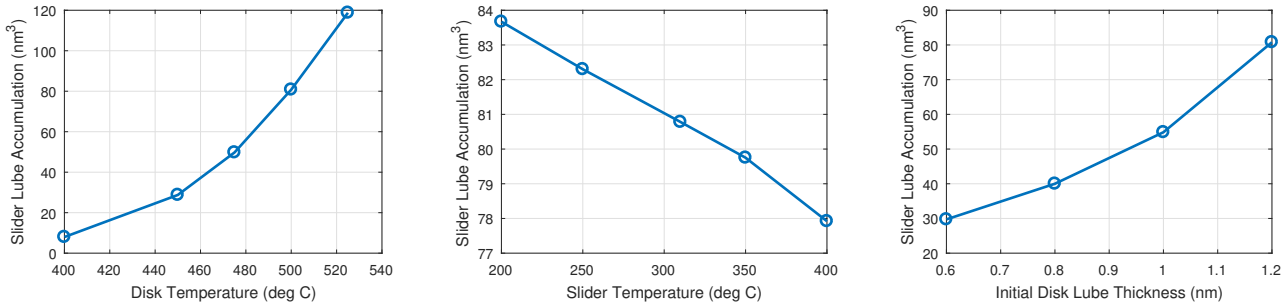

(a) Disk Temperature Study (b) Slider Temperature Study (c) Initial Lube Thickness Study

Fig. 8: Lubricant Accumulation on the slider (nm^3) as a function of disk temperature, slider temperature and initial lube thickness. Increase in the disk temperature and initial lubricant thickness causes the slider lube accumulation to rise. Change in head temperature has a minimal effect on the accumulation.

and slider temperatures are kept constant at 500°C and 310°C respectively. We consider four cases - (a) without convection and diffusion (b) with convection, without diffusion, (c) without convection, with diffusion and (d) with convection and diffusion. As shown the Figure 9, cases (a) and (b) (without diffusion, without/with convection) have similar solution profiles, as do cases (c) and (d) (with diffusion, without/with convection). Thus, the air convection model does not seem to have a significant effect on the lubricant transfer process. This can be justified by the following simple calculation. Kinetic energy of a vapor molecule is given by $\frac{1}{2}mv^2$, where $m = 2000 \times 1.66 \times 10^{27}$ kg for Zdol 2000. The thermal energy of a vapor molecule can be estimated as $\frac{3}{2}kT$, where k is the Boltzmann constant. Equating these at a disk temperature of 773 K, we find that the speed of a vapor molecule ejected from the disk is of the order of 100 m/s [41]. This is almost 8 times the disk velocity. Thus the rate of ejection of lubricant molecules is much higher than the rate of convection, which explains why air convection has a negligible impact on the lubricant transfer process. Diffusion, on the other hand, has a significant impact on the profile of the deposited slider lubricant film. For the cases where diffusion was ignored (a) and (b), the slider lubricant film has a much steeper slope and narrow width. Inclusion of the vapor diffusion effect causes the slider lubricant profile to spread out - the profile is wider but shorter in height, which is a direct consequence of the diffusion of the lubricant vapor pressure profile. However, the volume of accumulation in all four cases was found to be almost unchanged (less than 6% change).

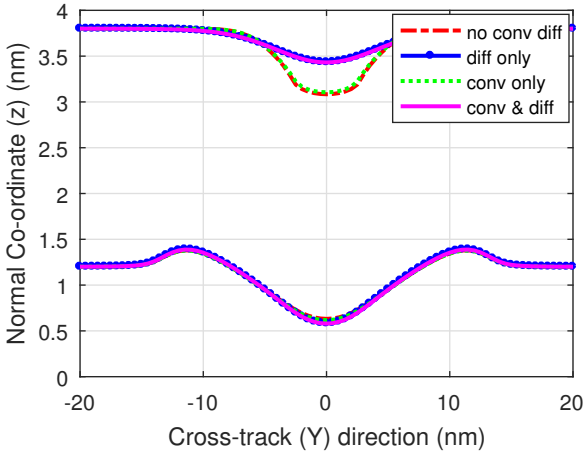

Fig. 9: Effect of convection and diffusion on lubricant profile on the disk and slider. Convection has a small effect on the profile, diffusion causes the accumulation profile to spread-out. $T_{max,d} = 500$ °C, $T_{max,s} = 310$ °C, $U_d = 12.5$ m/s, fh = 4 nm, FWHM = 20 nm, $t_f = 1$ ns. Origin ($X = 0$, $Y = 0$) is at NFT center.

3.6 Laser Spot Size Study

Here we study the effect of the laser spot size on the lubricant transfer process. We consider four thermal spot sizes - 20 nm, 50 nm, 100 nm and 1 μm. To directly compare the amount of slider lubricant accumulation during the 2 ns of laser illumination, a normalized volume quantity needs to be determined. We follow the method used by Dahl and Bogy [15] and define "normalized slider lubricant accumulation" as:

$$\overline{\Delta V}_{slider} \equiv \frac{\Delta V_{slider}}{L^2}$$

where ΔV_{slider} is the slider's lubricant accumulation defined in Section 3.2. Figure 10 plots the normalized

slider lubricant accumulation as a function of time for different spot sizes. For the shorter illumination time, $\overline{\Delta V}_{slider}$ for larger spot sizes is greater than that for smaller spot sizes. However, the trend reverses for larger simulation times. This implies that, on a relative scale, slider lubricant accumulation is more significant for larger spot sizes at small illumination times. However, for larger illumination times, slider lubricant accumulation is more significant for smaller spot sizes.

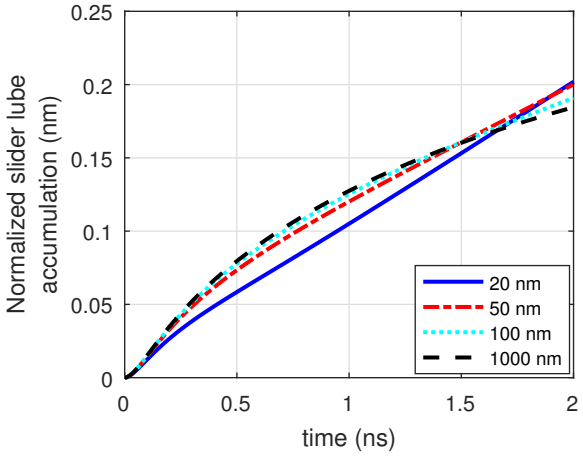

Fig. 10: Normalized lubricant accumulation on slider (nm^3) versus time for different Laser Spot Sizes. On a relative scale, small laser spot sizes show larger accumulation for long simulation times. $T_{max,s}$ = 310 °C, U_d = 12.5 m/s, fh = 4 nm, FWHM = 20 nm.

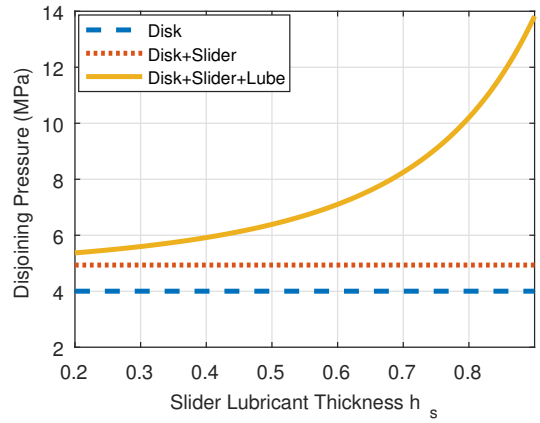

(a) Π_d

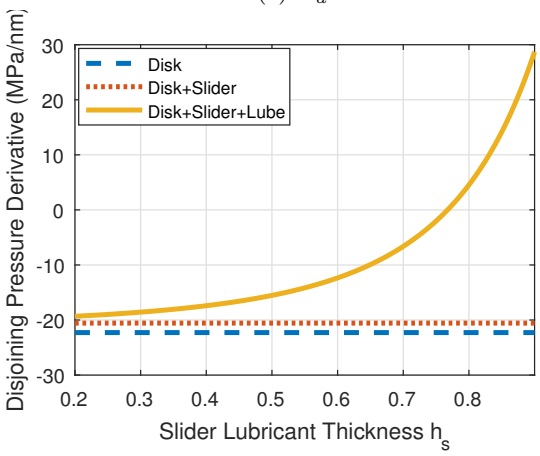

(b) $\frac{\partial \Pi_d}{\partial h_d}$

Fig. 11: Effect of Slider Lubricant Thickness (h_s) on Disk Disjoining Pressure. When lubricant-lubricant interactions are considered, both Π_d and $\frac{\partial \Pi_d}{\partial h_d}$ increase rapidly with h_s.

3.7 Disjoining Pressure Study (Mechanical Transfer)

As described in Eq. 4, the disk lubricant disjoining pressure Π_d depends on the disk lubricant thickness h_d, slider lubricant thickness h_s and the head-disk spacing fh. Figure 11 plots the variation of disk lubricant disjoining pressure Π_d and its derivative $\frac{\partial \Pi_d}{\partial h_d}$ with h_s at fh = 3 nm and h_d = 1.2 nm. When only the disk-lubricant and/or slider-lubricant interactions are considered, the disk disjoining pressure is independent of h_s. However, when lubricant-lubricant interactions are considered, as h_s increases, both Π_d and $\frac{\partial \Pi_d}{\partial h_d}$ increase. The increase in Π_d would result in the suppression of the evaporation rate from the disk according to Eq. 6 and 7. Figure 11 shows that $\frac{\partial \Pi_d}{\partial h_d}$ becomes 0 at h_s of 0.77 nm and is positive for larger h_s. Hence, we expect that dewetting of the disk lubricant film would occur beyond this stage of lubricant accumulation on the slider. As the slider lubricant accumulation increases with time, the rate of evaporation decreases, while the dewetting instability of the disk lubricant film increases. This causes a change in the lubricant transfer mechanism from thermal (evaporation/condensation driven) to mechanical or molecular interactions driven (dewetting instability driven).

In order to demonstrate this phenomenon, we illuminate the disk lubricant with a 20 nm FWHM thermal spot scanning at a speed of 12.5 m/s at a head-disk spacing of 3 nm. The maximum disk and slider temperatures are kept constant at 500°C and 310°C, respectively. We consider two cases - (a) Effect of Slider and Slider Lubricant on Disk Disjoining Pressure are ignored, (b) Effect of Slider and Slider Lubricant on Disk Disjoining Pressure are considered. Figure 12 plots the cross-track and down-track lubricant profiles for the disk and slider after of 1.5 ns of illumination. Until this stage, the amount of lubricant transfer from the disk to the slider

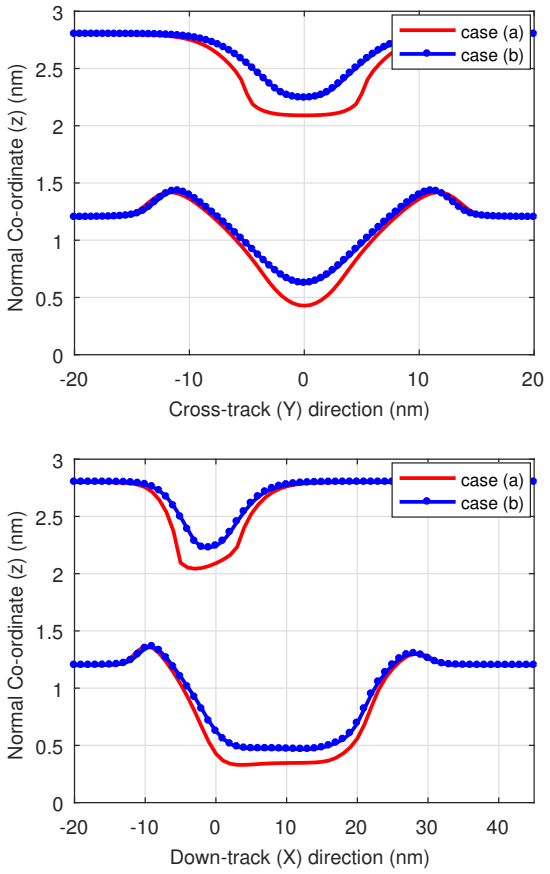

Fig. 12: Disjoining Pressure Study: Case (a) Only disk-lubricant interactions are considered, Case (b) disk-lubricant, slider-lubricant and lubricant-lubricant interactions are considered. Increase in Π_d when all interactions are considered causes the amount of lube transfer due to evaporation to decrease. $T_{max,d}$ = 500 °C, $T_{max,s}$ = 310 °C, U_d = 12.5 m/s, fh = 4 nm, FWHM = 20 nm, t_f = 1.5 ns. Origin ($X = 0$, $Y = 0$) is at NFT center.

is higher for case (a) than case (b). When the influence of the slider and slider lubricant on the disjoining pressure are considered (Case (b)), the evaporation rate is lower due to higher disjoining pressure, leading to less transfer by the "thermally activated" mechanism. If the illumination of the disk is continued beyond 1.5 ns, the disjoining pressure and its derivative both continue to increase (in case (b)) due to the increase in the slider's lubricant height. Finally, at a simulation time of 1.9 ns, the disjoining pressure derivative becomes 0. The simulation becomes unstable beyond this stage due to dewetting. Any small perturbations in the system would continue to grow, causing the simulation to blow up. If the laser illumination is continued beyond 1.9 ns, we expect a significant pick-up of the disk lubricant caused by the temperature gradient on a dewetting lubricant film.

A similar effect is observed on decreasing the head-disk spacing. Figure 13 plots the variation of Π_d and $\frac{\partial \Pi_d}{\partial h_d}$ with fh at h_s = 0.2 nm and h_d = 1.2 nm. When only the disk-lubricant interactions are considered, Π_d is independent of fh. However, when the slider-lubricant and lubricant-lubricant interactions are considered, as fh decreases, both Π_d and $\frac{\partial \Pi_d}{\partial h_d}$ increase; $\frac{\partial \Pi_d}{\partial h_d}$ becomes 0 at fh of around 2.5 nm. At relatively higher head-disk spacing ($\sim$ 4 nm), the disk to slider lubricant transfer mechanism is largely thermally activated. On the other hand, for lower head-disk spacings ($\sim$ 2.5 nm), the transfer mechanism is largely driven by dewetting instability.

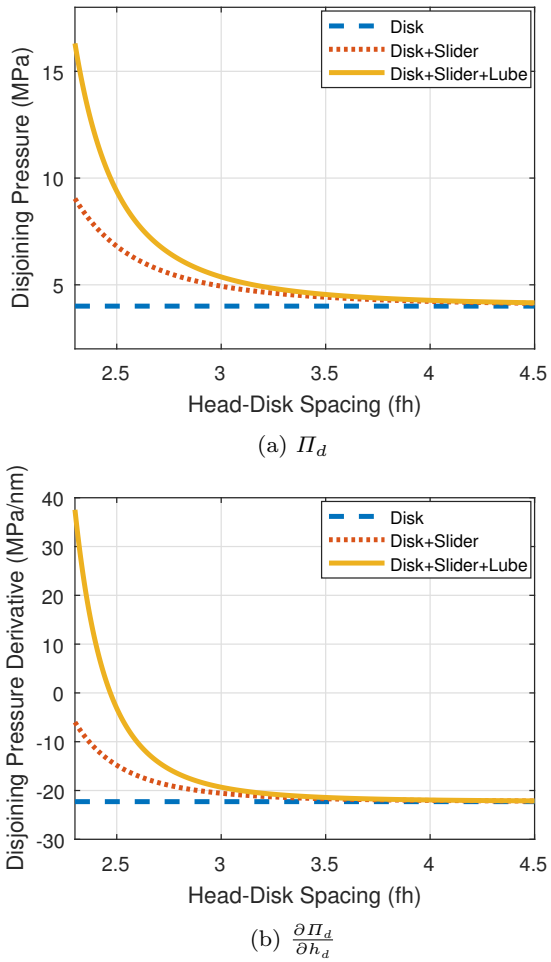

(a) Π_d

(b) $\frac{\partial \Pi_d}{\partial h_d}$

Fig. 13: Effect of Head-Disk Spacing (fh) on Disk Disjoining Pressure. When the slider-lubricant and lubricant-lubricant interactions are considered, both Π_d and $\frac{\partial \Pi_d}{\partial h_d}$ increase rapidly as h_s decreases.

4 Discussion

We have shown that several angstroms of lubricant accumulation on the slider is possible after 2 ns of disk lubricant illumination. At head-disk spacings of $\sim$ 3 - 4 nm, the head-disk lubricant transfer is initially largely caused by temperature difference driven evaporation/ condensation. Lubricant accumulation grows much more with increase in temperature. When an initial disk lubricant film of 1.2 nm is subjected to a maximum disk temperature of 400°C, the slider lubricant accumulation is merely 8 nm^3, whereas at a peak temperature of 525°C, the accumulated volume is 118.8 nm^3. Moreover, close to the HAMR target temperature, even small changes in the maximum disk temperature can help in reducing the lubricant transfer to the head. For example, reducing the peak temperature from 525°C to 500°C and further to 475 °C reduces the accumulated volume on the slider from 118.8 nm^3 to 80.8 nm^3 and further to 49.8 nm^3. The corresponding drop in the peak slider lubricant height is 1 nm to 0.85 nm and further to 0.65 nm for 525°C, 500°C and 475°C, respectively. While it was expected that a drop in media temperature would result in a lower transfer, the high sensitivity of the slope of the lubricant accumulation curve (Figure 8a) near the HAMR target temperature of 500 °C is a crucial insight towards managing lubricant and material transfer during HAMR writing.

Comparatively, the head temperature has a small impact on the amount of lubricant transfer. Variation in the maximum head temperature from a high of 400°C to a low of 200°C (with the disk being maintained at a peak temperature of 500°C) resulted in a rise in the slider lubricant accumulation from 77.9 nm^3 to only 83.7 nm^3. The corresponding variation in peak slider lubricant height is 0.77 nm to 0.97 nm. Thinner lubricant films have larger disjoining pressures and effective viscosities and are much more resistive to deformation and evaporation. Reducing the thickness of the initial lubricant film coated on the disk can also help in reducing the amount of lubricant pick-up.

While the lubricant transfer is initially dominated by evaporation/ condensation, as the amount of lubricant accumulation on the slider increases, the influence of the slider-lubricant and lubricant-lubricant molecular interactions becomes increasingly important. There exists a critical value of accumulated slider lubricant thickness at which the disjoining pressure derivative becomes zero and significant lubricant transfer is expected originating from dewetting instability. Figure 14a plots this critical slider lubricant thickness as a function of disk lubricant thickness at different head-disk spacings. We see that for higher disk lubricant thickness, the critical slider lubricant thickness for the onset of dewetting is lower. The critical slider lubricant thickness also decreases as the head-disk spacing is reduced. In fact, at very low head-disk spacings ($\sim$ 2.5 nm), lubricant dewetting occurs at almost no slider lubricant accumulation. This is highlighted in Figure 14b, which plots the critical head-disk spacing at which the dewetting of disk lubricant occurs without any accumulation of slider lubricant (h_s was set equal to 0.2 nm) as a function of disk lubricant thickness. At such low spacings, we expect to see lubricant pick-up even before the initiation of laser heating. This phenomenon was demonstrated experimentally by Ambekar et. al [10].

Few numerical studies have been presented in the literature on lubricant transfer in HAMR, however, those models may not be sufficiently accurate due to some unrealistic assumptions, such as a uniform disk lubricant film and uniform temperature distribution. Ma and Liu [7] studied lubricant transfer in HAMR without considering the effect of spatial temperature gradient on lube evolution. While their model qualitatively predicted that lube thinning rate increases dramatically with rise in temperature, they predicted significantly lower lube thinning rates - time for 1 nm disk lube in the area from 20 to 40 mm radius to uniformly thin 1Å was on the order of seconds for Zdol 2000 under a 100 nm laser spot at 450°C. Our model and previous works [15] predict several angstroms of local lube deformation and transfer in a time scale of nanoseconds due to spatial temperature variation at similar peak media temperatures and laser spot sizes.

In this study, we have not considered the effects of thermal decomposition or lubricant polydisperity. Experiments suggest that the thermal decomposition of Zdol occurs at temperatures above 600 K [42]. Hence, in addition to evaporation, thermal decomposition could be another potential mechanism contributing towards desorption of lubricant molecules from the disk at high temperatures. PFPE lubricants are not chemically pure materials, but rather are a mixture of different molecular weight components. Since the rate of evaporation is a strong function of molecular weight, the degree of polydisperity will determine how the evaporation rate varies as lighter molecules will evaporate first [43].

The same physics of molecular interactions and their changes with temperature applies to surface tension and interfacial energetics. Marchon and Saito [18] considered the effect of a temperature dependent Hamaker constant on lubricant thermo-diffusion under laser heating. The model developed here can be improved by considering the effect of temperature on the Hamaker constants A_{VLS}, A_{LVL} and A_{SVL}.

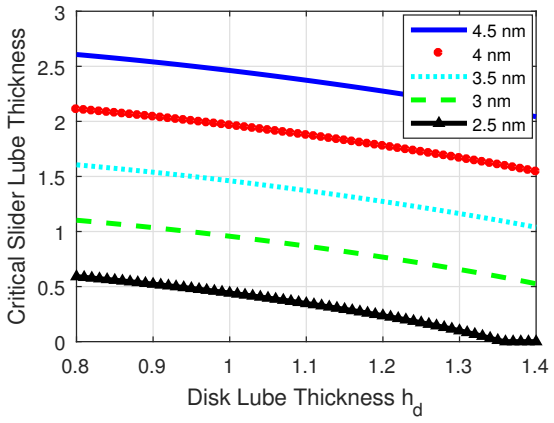

(a) Critical accumulated head lubricant thickness for the onset of dewetting versus disk lubricant thickness at different head-disk spacings. Critical head lube thickness decreases with an increase in the disk lube thickness and decrease in head-disk spacing.

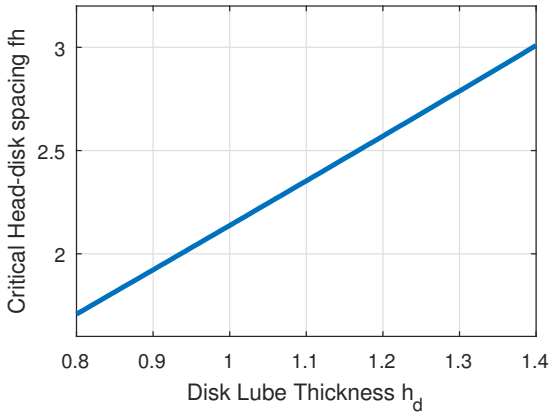

(b) Critical Head-disk spacing for the onset of dewetting instability as a function of disk lubricant thickness. At head-disk spacings below the critical value, lubricant pick-up is expected to occur even before the laser is turned on.

Fig. 14: Critical h_s and fh for onset of Dewetting Instability

The lubricant is assumed to be a viscous, Newtonian fluid in this study. In reality, PFPE lubricants exhibit viscoelastic behavior [32]. Sarabi and Bogy [44] studied the effect of lubricant viscoelasticity on disk lubricant evolution under HAMR laser heating. They found that the lubricant behaves more like a viscoelastic solid rather than a viscous fluid in the time scale and length scale of the HAMR laser heating problem. The model presented here can also be improved by considering viscoelastic effects on the lubricant transfer process.

The governing equation for the disk/slider lubricant film used in this study assumes a quasi-parallel film. Though the results presented are only for 2 ns of laser illumination, we performed simulations with this model for longer laser shine times ($\sim$ 10 ns). We found that as the amount of slider accumulation increases with time, the slope of the slider lubricant profile becomes very high, violating the quasi-parallel film assumption. In order to predict the lubricant transfer process for high volumes of accumulation, the governing equations need to be modified to allow high slopes. The expression for disjoining pressure also needs to be updated to consider the impact of film curvature [45].

5 Conclusion

We have developed a continuum mechanics based model that predicts the lubricant transfer from the disk to the slider during HAMR writing. The model simultaneously determines the deformation and evaporation of the lubricant film on the disk, the convection and diffusion of the vapor phase lubricant in the air bearing and the evolution of the condensed lubricant film on the slider. The model also accounts for molecular interactions between the disk-lubricant, slider-lubricant and lubricant-lubricant in terms of disjoining pressure. We found that at head-disk spacings of $\sim$ 3 - 4 nm, the head-disk transfer mechanism is initially largely thermally driven. Hence, the amount of lubricant accumulation on the slider can be significantly reduced by decreasing the media temperature. However, as lubricant accumulation increases with time, we see a change in the transfer mechanism from thermally driven to molecular interactions driven (dewetting instability). A similar change in transfer mechanism from thermal to mechanical is predicted as we reduce the head-disk spacing. There exists a critical value of head-disk spacing and a critical value of head lubricant height at which dewetting of the disk lubricant begins, leading to enhanced lubricant pick-up.

Acknowledgements This work was supported by the Computer Mechanics Laboratory at University of California, Berkeley, Mechanical Engineering Department. This is a post-peer-review, pre-copyedit version of an article published in Tribology Letters. The final authenticated version is available online at: http://dx.doi.org/10.1007/s11249-017-0952-3

References

1. Kryder, M., Gage, E., McDaniel, T., Challener, W., Rottmayer, R., Ju, G., Hsia, Y.T., Erden, M.: Heat assisted magnetic recording. Proceedings of the IEEE (2008). doi: 10.1109/JPROC.2008.2004315
2. Marchon, B., Guo, X.C., Pathem, B.K., Rose, F., Dai, Q., Feliss, N., Schreck, E., Reiner, J., Mosendz, O., Takano, K., Do, H., Burns, J., Saito, Y.: Head-disk interface materials

issues in heat-assisted magnetic recording. IEEE transaction on magnetics (2014). doi: 10.1109/TMAG.2013.2283068
3. Kiely, J.D., Jones, P.M., Y.Yang, Brand, J.L., Anaya-Dufresne, M., Fletcher, P.C., Zavaliche, F., Toivola, Y., Duda, J.C., Johnson, M.T.: Write-induced head contamination in heat-assisted magnetic recording. IEEE transactions on magnetics (2017). doi: 10.1109/TMAG.2016.2618842
4. Xiong, S., Wang, N., Smith, R., Li, D., Schreck, E., Dai, Q.: Material transfer inside head disk interface for heat assisted magnetic recording. Tribol Lett (2017). doi: 10.1007/s11249-017-0860-6
5. Marchon, B., Karis, T., Dai, Q., Pit, R.: A model for lubricant flow from disk to slider. IEEE transactions on magnetics (2003). doi: 10.1109/TMAG.2003.816433
6. Ma, Y., Liu, B.: Dominant factors in lubricant transfer and accumulation in slider-disk interface. Tribol Lett (2008). doi: 10.1007/s11249-007-9289-7
7. Ma, Y., Liu, B.: Lube depletion caused by thermal-desorption in heat assisted magnetic recording. IEEE transactions in magnetics (2008). doi: 10.1109/TMAG.2008.2001670
8. Yang, Y., Li, X., Stirniman, M., Yan, X., Huang, F., Zavaliche, F., Wang, H., Huang, J., Tang, H., Jones, P.M., Kiely, J.D., Brand, J.L.: Head disk lubricant transfer and deposition during heat-assisted magnetic recording write operations. IEEE transactions on magnetics (2015). doi: 10.1109/TMAG.2015.2434826
9. Wu, L.: A model for liquid transfer between two approaching gas bearing surfaces through coupled evaporation-condensation and migration dynamics. Journal of Applied Physics (2008). doi: 10.1063/1.2951616
10. Ambekar, R.P., Bogy, D.B., Dai, Q., Marchon, B.: Critical clearance and lubricant instability at the head-disk interface of a disk drive. Applied Physics Letters (2008). doi: 10.1063/1.2837187
11. Mate, C.M.: Taking a fresh look at disjoining pressure of lubricants at slider-disk interfaces. IEEE transaction on magnetics (2011). doi: 10.1109/TMAG.2010.2073691
12. Waltman, R.J., Deng, H., Wang, G.J., Zhu, H., Tyndall, G.W.: The effect of PFPE film thickness and molecular polarity on the pick-up of disk lubricant by a low-flying slider. Tribol Lett (2010). doi: 10.1007/s11249-010-9638-9
13. Zhang, Y., Polycarpou, A.A.: Lubricant transfer model at the head-disk interface in magnetic storage considering lubricant lubricant interaction. Tribol Lett (2016). doi: 10.1007/s11249-016-0688-5
14. Li, N., Meng, Y., Bogy, D.B.: Effects of PFPE lubricant properties on the critical clearance and rate of the lubricant transfer from disk surface to slider. Tribol Lett (2011). doi: 10.1007/s11249-011-9806-6
15. Dahl, J.B., Bogy, D.B.: Lubricant flow and evaporation model for heat-assisted magnetic recording including functional end-group effects and thin film viscosity. Tribol Lett (2013). doi: 10.1007/s11249-013-0190-2
16. Wu, L.: Modelling and simulation of the lubricant depletion process induced by laser heating in heat-assisted magnetic recording system. Nanotechnology (2007). doi:10.1088/0957-4484/18/21/215702
17. Wu, L., Talke, F.E.: Modeling laser induced lubricant depletion in heat-assisted-magnetic recording systems using a multiple-layered disk structure. Microsyst Technol (2011). doi: 10.1007/s00542-011-1300-4
18. Marchon, B., Saito, Y.: Lubricant thermodiffusion in heat assisted magnetic recording. IEEE transaction on magnetics (2012). doi: 10.1109/TMAG.2012.2194138
19. Sarabi, M.S.G., Bogy, D.B.: Simulation of the performance of various PFPE lubricants under heat assisted magnetic recording conditions. Tribol Lett (2014). doi: 10.1007/s11249-014-0409-x
20. Mendez, A.R., Bogy, D.B.: Lubricant flow and accumulation on the sliders air-bearing surface in a hard disk drive. Tribol Lett (2014). doi: 10.1007/s11249-013-0285-9
21. Oron, A., Davis, S., Bankoff, S.: Long-scale evolution of thin liquid films. Rev. Mod. Phys. (1997). doi: 10.1103/RevModPhys.69.931
22. Batchelor, G.: An Introduction to Fluid Dynamics. Cambridge University Press, Cambridge, England (1967)
23. Derjaguin B.V., Churaev N., Muller V. Surface Forces. Consultants Bureau, Plenum Publishing Corporation, New York (1987)
24. Karis, T., Tyndall, G.: Calculation of spreading profiles for molecularly-thin films from surface energy gradients. Journal of non-newtonian fluid mechanics (1999). doi: 10.1016/S0377-0257(98)00167-0
25. Tyndall, G., Leezenberg, P., Waltman, R., Castenada, J.: Interfacial interactions of perfluoropolyether lubricants with magnetic recording media. Tribology Letters (1998). doi: 10.1023/A:1019199004170
26. Pit, R., Marchon, B., Meeks, S., Velidandla, V.: Formation of lubricant moguls at the head/disk interface. Tribology Letters (2001). doi: 10.1023/A:1009074007241
27. Derjaguin, B., N, C.: Polymolecular adsorption and capillary condensation in narrow slit pores. Progress in Surface Science (1992). doi: 10.1016/0079-6816(92)90045-J
28. Forcada, M.: Instability in a system of two interacting liquid films: Formation of liquid bridges between solid surfaces. The Journal of Chemical Physics (1993). doi: 10.1063/1.464606
29. Christenson, H.: Capillary condensation due to vander waals attraction in wet slits. Physical Review Letters (1994). doi: 10.1103/PhysRevLett.73.1821
30. Israelachvili, J.N.: Intermolecular and surface forces: revised third edition. Academic press (2011)
31. Karis, T., Marchon, B., Flores, V., Scarpulla, M.: Lubricant spin-off from magnetic recording disks. Tribology Letters (2001). doi: 10.1023/A:1012553415639
32. Karis, T.: Lubricants for the disk drive industry. In: Rudnick L. (eds) Lubricant Additives: Chemistry and Applications, chap 22. CRC Press, Boca Raton, FL, pp. 523584 (2009)
33. Carey, V.P.: Liquid-Vapor Phase-Change Phenomena, 2 edn. Taylor and Francis Group, LLC, New York (2008)
34. Rosenblatt, G.M.: Evaporation from Solids. In: N. Hannay (eds) Treatise on Solid State Chemistry, vol. 6A, chap. 3. Plenum Press, New York, pp. 165240 (1976)
35. Wu, L.: Lubricant dynamics under sliding condition in disk drives. Journal of Applied Physics (2006). doi: 10.1063/1.2220489
36. Dahl, J.B., Bogy, D.B.: Static and Dynamic Slider Air-Bearing Behavior in Heat-Assisted Magnetic Recording Under Thermal Flying Height Control and Laser System-Induced Protrusion. Tribol Lett (2014). doi: 10.1007/s11249-014-0305-4
37. Hirschfelder, J.O., Bird, R.B., Spotz, E.L.: The transport properties of gases and gaseous mixtures. ii. Chem. Rev. (1949). doi: 10.1021/cr60137a012
38. Patankar, S.: Numerical Heat Transfer and Fluid Flow. Hemisphere Publishing Corporation, New York (1980)
39. Yabe, T., Aoki, T., Sakaguchi, G., Wang, P.: The compact CIP (cubic-interpolated pseudo particle) method as a general hyperbolic solver. Computers & Fluids (1991). doi: 10.1016/0045-7930(91)90067-R
40. Aoki T.: Multi-dimensional advection of CIP (cubicinterpolated propagation) scheme. Comput. Fluid Dyn. J. 4(3), 279-291, 1995

41. Jones, P.M., Yan, X., Hohlfeld, J., Stirniman, M., Kiely, J.D., Zavaliche, F., Tang, H.H.: Laser-induced thermodesorption of perfluoropolyether lubricant from the surface of a heat-assisted magnetic recording disk: Lubricant evaporation and diffusion. Tribol Lett (2015). doi: 10.1007/s11249-015-0561-y
42. Lei, R.Z., Gellman, A.J., Jones, P.: Thermal stability of fomblin z and fomblin zdol thin lms on amorphous hydrogenated carbon. Tribology Letters (2001). doi: 10.1023/A:1016670303657
43. Zhou, W., Zeng, Y., Liu, B., Yu, S., Hua, W., Huang, X.: Evaporation of polydisperse perfluoropolyether lubricants in heat-assisted magnetic recording. Appl. Phys. Express (2011). doi: 10.1143/APEX.4.095201
44. Sarabi, S., Bogy, D.B.: Viscoelastic effects on lubricant depletion and recovery under heat-assisted magnetic recording (HAMR) conditions. ASME Information Storage and Processing Systems (2016). doi: 10.1115/ISPS2016-9578
45. Dai, B., Leal L.G., Redondo A.: Disjoining pressure for nonuniform thin films. Physical Review E (2008). doi: 10.1103/PhysRevE.78.061602